Journal of Magnetism and Magnetic Materials 476 (2019) 268–273

Contents lists available at ScienceDirect

Journal of Magnetism and Magnetic Materials

journal homepage: www.elsevier.com/locate/jmmm

Research articles

Mechanism of high temperature induced phase transformation and magnetic properties of Mn_3O_4 crystallites

Lakshmi Narayani[a], V. Jagadeesha Angadi[b,*], Anu Sukhdev[b,*], Malathi Challa[c], Shidaling Matteppanavar[d], P.R. Deepthi[b], P. Mohan Kumar[b], Mehaboob Pasha[b]

[a] Department of Chemistry, MES PU College, Bengaluru 560012, India
[b] Material Research Center, School of Engineering, Presidency University, Bengaluru 560064, India
[c] Department of Chemistry, Ramaiah Institute of Technology, Bengaluru, India
[d] New Chemistry Unit, Jawaharlal Nehru Center for Advanced Scientific Research, Bangalore 560064, India

ARTICLE INFO

Keywords:
Bixbyite
Hausmannite-phase transition
Solution combustion synthesis
Urea
Glucose
Susceptibility

ABSTRACT

This paper is an experimental study of the different phases of oxides of manganese, prepared by solution combustion method using mixture of urea and glucose as fuels. To validate the thermal stability of Mn_2O_3, the as-synthesized sample was subjected to heat treatment from 350 °C to 1000 °C with 100 °C interval. The change in Mn_2O_3 to Mn_3O_4 was identified by powder X-ray diffraction (PXRD) to show the temperature dependent phase transformation that occur during the heat treatment process. The PXRD patterns show that Mn_2O_3 is stable between temperatures of 350 °C to 850 °C, and a new phase i.e Mn_3O_4 appears at 1000 °C. The Mn_2O_3 and Mn_3O_4 have their distinct surface morphologies viz., spherical and rod shapes. The detailed morphology, elemental compositions and structure investigation were carried out by using Scanning Electron Microscopy (SEM-EDAX) and Raman spectroscopy. Sintered sample of Mn_3O_4 were subjected to magnetic measurements. The Mn_3O_4 crystallite with diameters of 50 nm shows ferromagnetic behavior with a phase transition from ferromagnetic to paramagnetic phase at 48 K. A large coercivity up to 3000 Oe and a small remanence of 0.1092 emu/g at 10 K, was observed. The temperature dependent magnetization measured in a magnetic field of 100 Oe, increases significantly with decreasing temperature around 45 K, both for the FC and ZFC measurements. The susceptibility measurement of the Mn_3O_4 crystallites were investigated between 0 and 300 K by applied magnetic fields up to 5 T. A magnetic transition is observed near 48 K which is attributed to the formation of the ferrimagnetic Mn_3O_4.

1. Introduction

Manganese oxide nano crystals have gained significance due to their fascinating structural, microstructural, dielectric and magnetic properties [1–5]. Their applications range from catalysis [7], biosensors [8], energy and magnetic data storage [9], Environmental protection [10], gas adsorption [11], catalysis [12]. photo catalysis [13], and magnetic resonance imaging [14]. Oxides of manganese are available in various oxidation states (2+, 3+, 4+, 5+, 6+, 7+). The most common oxides are MnO, MnO_2, Mn_2O_3, Mn_2O_5, MnO_3, Mn_2O_7 and many non-stoichiometric phases of Mn_3O_4. Bixbyite (Mn_2O_3) has been the focus of recent studies due to their structural and magnetic properties [15]. The structure of Mn_2O_3 is a slightly distorted version of the bixbyite structure, exhibiting both orthorhombic and cubic structures. The negative temperature coefficient (NTC) of Mn_2O_3 is leveraged for thermistors, oxidation catalysis and to produce super-paramagnetic materials [16]. Hausmannite (Mn_3O_4) is one of the most stable oxides and has a normal spinel structure. It is a mixed oxide containing both di- and tri-valents of Mn. There are 32 oxygen and 24 cations available in a unit cell. Hence it attracts special interest due to its unique oxidative behaviour. It is also used as a raw material for the preparation of electrode (Li–Mn–O) for rechargeable lithium batteries and soft magnetic materials such as Mn-Zn ferrite for transformer cores [17]. The bulk material of Mn_3O_4 is ferromagnetic behavior below 42 K, and is paramagnetic at room temperature. Due to the triangular arrangement of the magnetic moments, it behaves as a canted ferromagnetic [18,19]. To exploit the physico-chemical properties in the wide range of technological applications, it is necessary to explore novel methods for synthesis. There are many methods available to synthesize the manganese oxide nano particles such as precipitation method [20], solid state [21], hydrothermal

* Corresponding authors.
E-mail addresses: jagadeeshaangadi@presidencyuniversity.in (V. Jagadeesha Angadi), anu.sukhdev@presidencyuniversity.in (A. Sukhdev).

https://doi.org/10.1016/j.jmmm.2018.12.072
Received 23 October 2018; Received in revised form 14 December 2018; Accepted 17 December 2018
Available online 18 December 2018
0304-8853/

synthesis [22], reflux [21], sol gel [23] and thermal decomposition method [24] but limited reports on the phase transformation of oxides of manganese [25,26]. Amongst all the methods, solution combustion synthesis route is simple and economically feasible, which allows the production of fine, homogeneous crystalline nanoparticles. However, there are only few studies on the synthesis of oxides of manganese via combustion route. Therefore, we are reporting for the first time, the temperature dependent phase transformation of oxides of manganese between 350 °C and 1000 °C, by adopting a combustion method that uses a mixture of urea and glucose as fuels. Structural, Microstructural, Raman spectroscopy and susceptibility measurement were studied to understand crystallinity, phase, structure, morphology, elemental composition details, thermal stability, phase transformation and magnetic behavior of Mn_3O_4.

2. Experimental method

2.1. Materials and reagents used for synthesis

Preparation of the Mn_3O_4, the Manganese(II) Nitrate tetrahydrate $[Mn(NO_3)_2{\cdot}4H_2O]$ (Merck, India with 99.9% purity), urea $[NH_2CONH_2]$ and glucose $[C_6H_{12}O_6)]$(Alfa, India) are taken.

2.2. Sample preparation

The oxidizer and mixture of glucose and urea are evaluated based on the oxidizing and reducing valences of the compounds i.e 1: (60:40). For making the solution, double De-ionized water is used for making clear homogeneous solution. Further, chemicals of analytical grade with 99.9% purity were used. Manganese nitrate and mixture of fuels are diluted with 20 ml double De-ionized water and mixed thoroughly with the help of a magnetic stirrer with 750 rpm about 30 min to get a homogenous solution. The solution which contains redox mixture was taken in a beaker (250 ml) and kept in a pre-heated muffle furnace maintained at 350 ± 10 °C. Initially, the solution boils, then froths and ignites to yield fine black colored product. The process is completed within 30 min [27]. The chemical equation, flow chart of synthesis and steps of the chemical reaction of combustion method is shown below:

$$6Mn(NO_3)_2 + 2C_6H_{12}O_6 + NH_2CONH_2 = 3Mn_2O_3 + 13CO_2 + 7N_2 + 14H_2O\ (350^oC)$$

$$9Mn(NO_3)_2 + 3C_6H_{12}O_6 + 2NH_2CONH_2 = 3Mn_3O_4 + 20CO_2 + 11N_2 + 22H_2O\ (1000^oC)$$

2.3. Characterizations

As-synthesized samples was subjected to characterization by powder X-ray diffraction (XRD) using Shimadzu 7000 powder diffractometer with Cu-Kα, radiation (λ = 1.5406 Å) in the range 10° ≤ 2θ ≤ 80°. To study the crystallinity, phase and structure. As prepared samples is subjected to heat treatment process from 350 to 1000 °C with an interval of 100 °C. From the XRD results, we have confirmed the formation of Mn_2O_3 phase up to 900 °C and around 1000 °C, Mn_3O_4 phase was formed without any impurity phase. Hence further characterizations was carried out for 1000 °C sintered sample.

The surface morphology and elemental analysis was done by using "Ultra 55 Scanning Electron Microscope" with an electron energy of 5 kV. Further Raman scattering measurements were carried out by JY Horiba LabRAM HR instrument to understand the spectroscopic properties of the samples.

The temperature dependence of the magnetization was carried out at different temperatures i.e 0–300 K for zero field-cooling (ZFC), the sample was cooled from room temperature to 0 K in the absence of external magnetic field 100 Oe. The magnetization as a function of temperature was recorded with increasing temperature. For field-cooling (FC), the sample was cooled from 300 to 0 K in the presence of an external magnetic field i.e B = 100 Oe, and the magnetization as a function of temperature was recorded with increasing temperature. Further, hysteresis loops of Mn_3O_4 crystallite were measured at different temperatures 10 and 100 K, respectively, with an applied magnetic field of 5 T to the Mn_3O_4 crystallites (see Figs. 1 and 2).

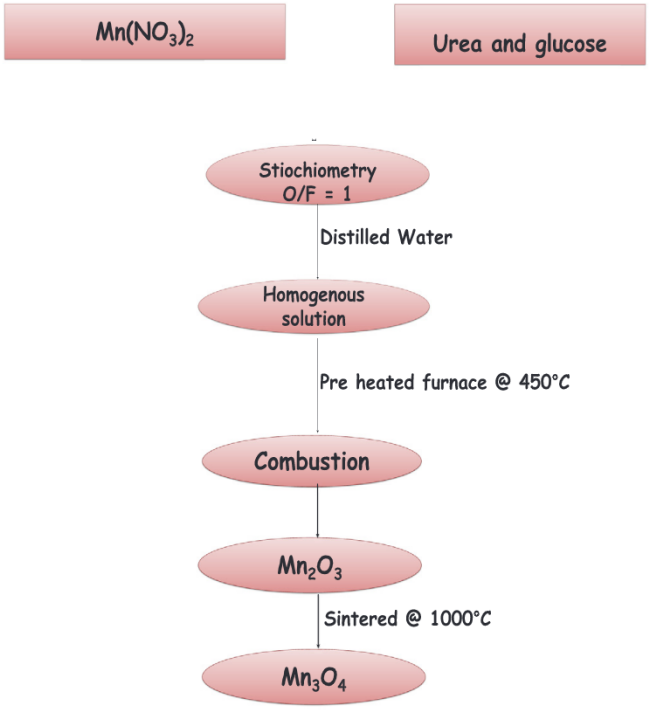

Fig. 1. Flow chart of synthesis by solution combustion route.

Fig. 2. Steps of the chemical reaction of combustion method.

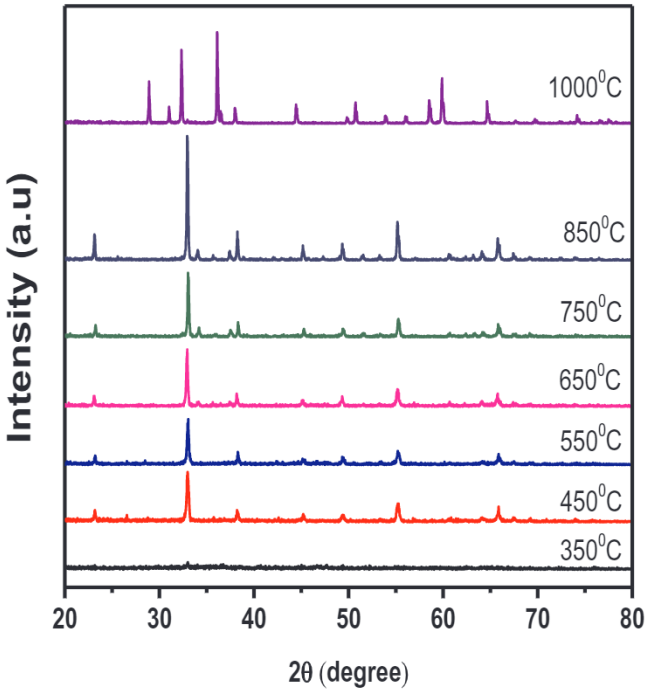

Fig. 3. XRD patterns of Mn_2O_3 (350–850 °C) thermal stability of Mn_2O_3, and transition from Mn_2O_3 to Mn_3O_4.

3. Results and discussions

3.1. Powder X-ray diffraction analysis

Fig. 3 represents the XRD pattern of the dried powdered samples calcined at different temperatures from 350 °C to 1000 °C with an interval of 100 °C. XRD peaks obtained at 350 °C to 850 °C was consistent with the reference JCPDS card No. 00-071-0635 and it is confirms refinement i.e Mn_2O_3 phase. The PXRD patterns of the products calcined up to 850 °C were similar which clearly indicates that Mn_2O_3 phase was thermally stable up to 850 °C. As the temperature of calcination increases, an extra peak appears at 34.1 (1 0 3) which is evident in the graph of 750 °C. The intensity of the peak increases with an increase in temperature and a sharp peak is observed at 1000 °C and these results are in accordance with JCPDS card 00-001-1127 hence, it is identified as Mn_3O_4 [27] phase. Further, these results were confirmed by Rietveld refinement of XRD data calcination at 1000 °C which was depicted in Fig. 4. The results suggested that Mn_2O_3 phases was well stable up to the 850 °C and it was completely transformed into Mn_3O_4 at 1000 °C (see Fig. 5). Therefore, we conclude that solution combustion method is the best method to prepare Mn_2O_3. Further, the structure of Mn_3O_4 is extracted from Rietveld refinement data and is shown in Fig. 6. The phase transformation temperature is not in agreement with previous reports and it can be attributed to the different synthetic method. The average crystallite size of Mn_2O_3 and Mn_3O_4 are calculated using the Debye Scherrer approximation i.e.

$$D_m = \frac{0.9\lambda}{\beta(\cos\theta)} nm \quad (1)$$

where D_m – average crystallite size, λ – wavelength (X-ray), β-is FWHM (full width with half maximum) and θ – angle of diffraction. The average crystallite size ranges from 35 to 55 nm as temperature varies. This may be due to agglomeration crystallite size during the phase transformation of Mn_2O_3 to Mn_3O_4 [28]. The lattice parameter was found to be increasing with an increase in the temperature range from 350 to 1000 °C i.e 9.401 Å to 9.456 Å. These results were depicted in Table. 1 and these are in good agreement with the reported values.

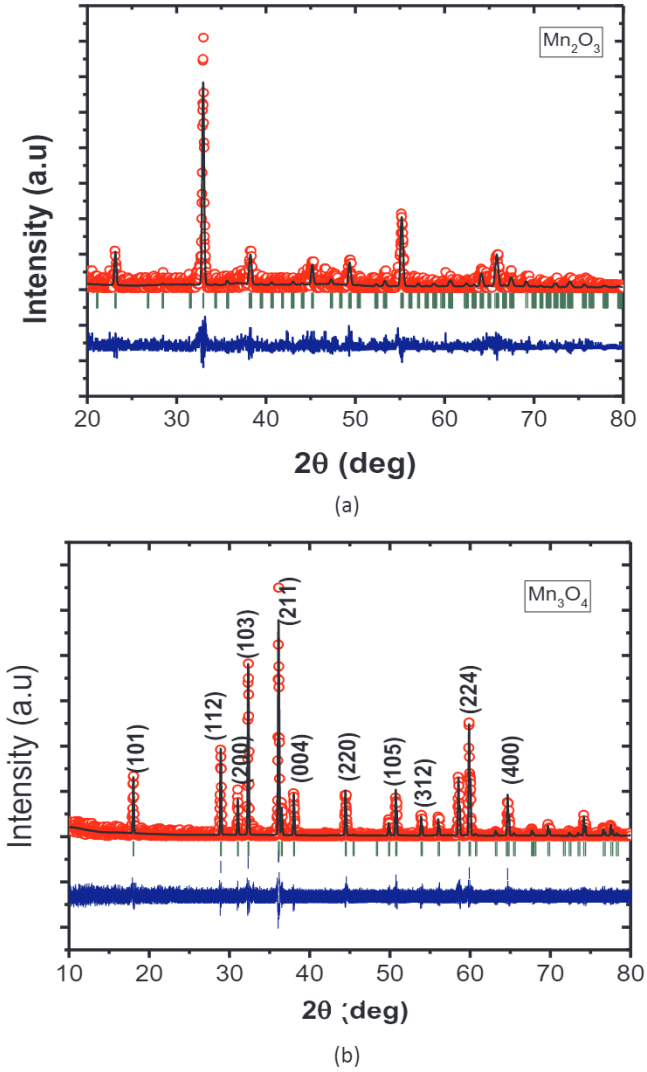

Fig. 4. (a-b). Refinement of Mn_3O_4 and Mn_2O_3sintered at 1000 and 450° centigrade.

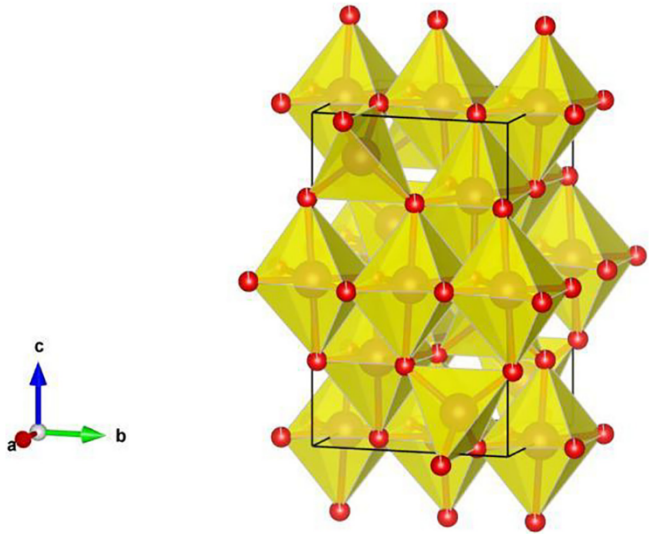

Fig. 5. Structure of Mn_2O_3 extracted by refinement.

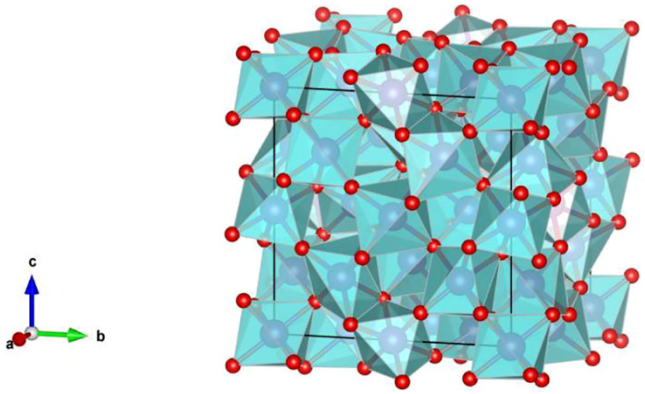

Fig. 6. Structure of Mn_3O_4 extracted by refinement.

Between the two values, it is observed that the lattice parameter (a) for Mn_3O_4 is larger which is indicates that the crystallite size is grown and suggests to the formation of new kind of surface morphology.

3.2. Morphology analysis by using SEM

The SEM micrographs of the samples at 350 and 1000 °C are depicted in the Fig. 7(a-b). At 350 °C, the sample is apparently uniform spheres in shape. Moreover, careful observation of micrographs, the Mn_2O_3 are in agglomeration of much smaller in size. With an increase in temperature, around 1000 °C, spherical particles of Mn_2O_3 are converted to rod shape structure due to heat treatment and the sample was identified as Mn_3O_4 from XRD. The formation of rods is the evidence from XRD analysis, suggesting the anisotropic growth in samples in one direction, since the base peak was found to be more dominant over the others, as well as the lattice parameter 'a' [21]. EDX spectra of samples at 350 °C and 1000 °C (Fig. 7(a) and (b)) represents the presence of Mn and O. Moreover, there were no reports available on Mn_2O_3 with rod type of surface morphology. Noteworthy, in this study is the preparation of two oxides of Mn with distinct surface morphology via solution combustion method using mixture of fuel reported for the first time.

3.3. Laser Raman spectroscopy (LRS).

Fig. 8 indicates Raman spectroscopy of Mn_3O_4. From the Fig. 8, we have observed 3 phonon high intense and doubly degenerate peaks, T2g symmetric mode at 366 cm^{-1}, Eg symmetric mode at 320 cm^{-1} and single degenerate A1g symmetric mode at 654 cm^{-1}, respectively. The band representing at 655 cm^{-1} was due to the stretching vibration of Mn-O in Mn_3O_4 oxides. At 350 °C, there is one more band T2g symmetry mode was exhibited at 487 cm^{-1}, which is due to out of plane bending mode of Mn_2O_3 phase [28]. The absorption band observed around 1038 cm^{-1} and 1162 cm^{-1} are assigned to the Mn-OH bending mode which belongs to the Au and Eu modes. The peak represented at 651 cm^{-1} belongs to Au mode and it is the characteristic peak of Mn_3O_4 molecule. This band represents the stretching vibrations of Mn-O bond.

3.4. Magnetic properties of Mn_3O_4

3.4.1. Dependence of temperature on magnetization.

Fig. 9 represents susceptibility measured in the magnetic field in the range of 100 Oe, increases subsequently with decreasing temperature for the FC and ZFC. In order to justify the reason for this behaviour, we shortly inspect the magnetic studies of manganese in the different crystallographic alterations and its oxides. It is reported in the literature that the Tc of Mn_3O_4 is 43 K and it is a ferrimagnetic substance with Tc = 43 K [27]. But in our report, Tc is found to be around 48 K. The ZFC curves measured in 100 Oe, exhibits its highest magnetization at 45 K. The negative shift of the peak in the ZFC curves with an enhancement of magnetic field helps in the frozen spins to overcome the energy fencer of the anisotropy. Blocking temperature (T_B) is the temperature where there is a highest magnetization in the ZFC curve. As identified by Néel, antiferromagnetic nanoparticles can show superparamagnetic relaxation of their spin lattices [26]. In comparison to ferromagnetic and ferrimagnetic nanoparticles, antiferromagnetic spins on nano scale may pose the superparamagnetic relaxation. The present Mn nanoparticles are a mixture of antiferromagnetic and ferrimagnetic Mn_3O_4. The ZFC-curve peak might also be the result of the mixture of results of the above phases. The maximum in the ZFC curves may be considered as an average T_b. In the present case, Mn nanoparticles does not exhibit any variation in magnetization from paramagnetic to antiferrimagnetic transition temperatures of a -Mn, MnO, MnO_2 or Mn_2O_3, which are represented in Fig. 6. The ZFC and FC curves which were studied at 0.02 T, do not coincide up to 240 K, which is greater than T_b and greatest of the PM-AFM transition temperatures of the phases (except-Mn) in Mn nanoparticles.

3.4.2. Magnetic field dependence of the magnetization

Fig. 10 depicts the M-H loops of Mn_3O_4 recorded at temperatures of 10 and 100 K, under the magnetic field of 5 T. The antiferro- and ferrimagnetic phases in the system contributes to the total magnetization. Generally, the contribution of antiferromagnetic phases shall be in small compared to the total magnetization. However, in the present study, antiferromagnetic phases are in nanoscale, hence, uncompensated spins at the surfaces of these particles results to a net moment, as stated by Neel [26]. The atomic chaos and canted spins of the surface atoms can also be the reason for the net magnetic moment. Generally, the magnetization of Mn_3O_4 nanoparticles in the field decreases with increasing temperature, a similar phenomenon, can be seen with the existing samples. We surmise that the magnetization depletion below 10 K may be due to inter particle interactions between the ferrimagnetic nanoparticles in the system. The M-H loops at 10 K, and 100 K show irreparable magnetization in fields up to 5 T. Moreover, even magnetic field of 5 T is not sufficient to saturate the sample. The high field differential susceptibility might indicate the possible existence of spin-glassy behaviour in the sample. The coercive field at 10 K is nearly 3000 Oe. This may be due to the small crystallite size of ferrimagnetic Mn_3O_4. The increase in the coercive field due to a similar reason can be observed in ferromagnetic Fe-nanoparticles [28]. Conceivably, the nanoparticles of various antiferromagnetic phases in the Mn_3O_4, also contribute to the coercive field. The extrapolation of the above equation to zero coercivity is acknowledged with the magnetic transition temperature of Mn_3O_4. The M-H loop clearly shows the clear transition of Mn_3O_4 ferri to paramagnetic behavior at around 100 k.

3.5. Conclusions

The synthesis of Mn_2O_3 prepared by solution combustion method using mixture of urea and glucose as fuels was reported for the first

Table 1
Structural parameters of Mn_2O_3 and Mn_3O_4 samples, obtained Rietveld refinement.

Temperature	Crystalline Phase (s)	L t.i·e 3.rau:	L:.t.i·e Par meters [A°]	average crysta lit. size (nm)	crystal syst· m	Morphology
3ɔ0 °C	M· ₂O₃	0.16:5	a = b = c – 9. .09i	3c.4	cubic	spherical
ı000 °C	Mn ₁O₄	14.33	a = b = ɔ.763; C = 9.456	ɔɔ.8	tetragonal	rod

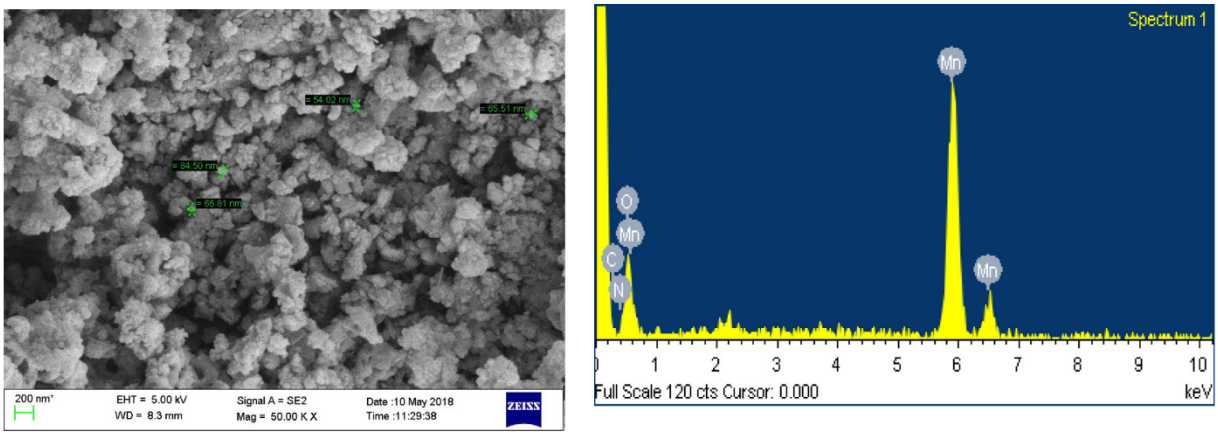

Fig. 7. (a-b). SEM micrograph of Mn_2O_3 and Mn_3O_4 nanoparticle.

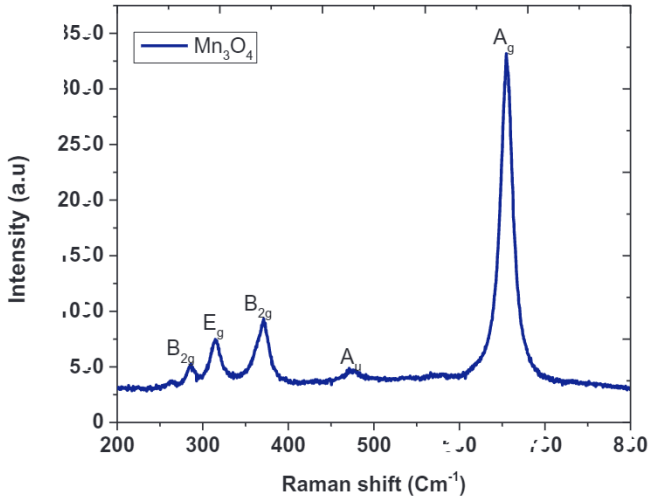

Fig. 8. Laser Raman Spectra of Mn_3O_4 nano crystals.

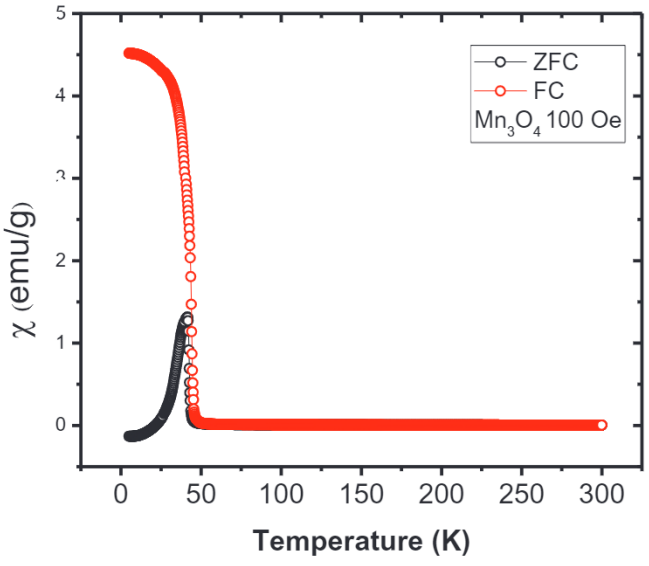

Fig. 9. ZFC-FC curve of Mn_3O_4 nanoparticles at 100 Oe,

time. The presence of Mn_2O_3 phase in the Mn nanoparticles was proved by XRD at 350, 450, 550, 650, 750 and 850 °C. A clear phase transition from Mn_2O_3 to Mn_3O_4 at 1000 °C was observed. It was also confirmed by FTIR and SEM results. The SEM results proves that most of the Mn_2O_3 crystals are irregular in shape and are of rough surfaces. The magnetic properties of Mn nanoparticles have been recorded in the range of 0–350 K under applied magnetic field till 5 T. The magnetic transition was observed near 48 K is assigned to the formation of the ferrimagnetic Mn_3O_4. The threshold process was observed below T_B. The intensity magnetization was not saturated even after applying the magnetic field of 5 T. The high coercive filed arises mainly from Mn_3O_4 phase transition and decreases linearly with increasing temperature

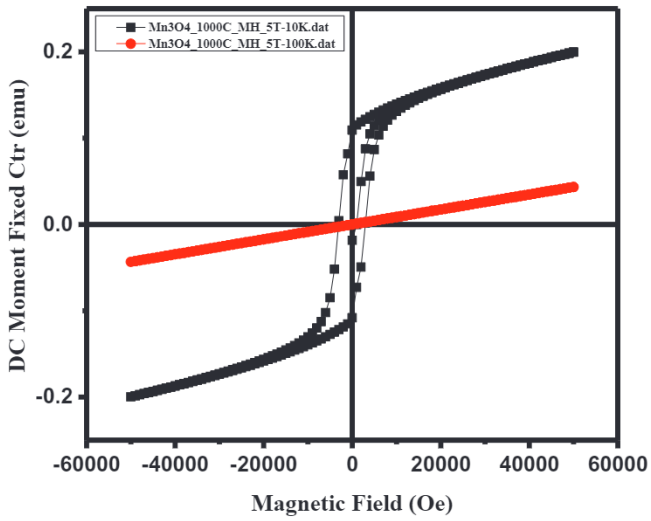

Fig. 10. Magnetization curve of Mn_3O_4 at 10 K and 100 K.

below 100 K. The relation of the magnetic properties and structure phase transition were studied elaborately.

Acknowledgement

The authors are thankful to the management of Presidency University, Bengaluru, for providing financial support through the University seed grant (File No: RI&C/Funded Project/RC1 dated 11/7/2018).

Appendix A. Supplementary data

Supplementary data to this article can be found online at https://doi.org/10.1016/j.jmmm.2018.12.072.

References

[1] Xiaodong Zhang, Hongxin L., Xut.an Lv, Xu. J.ngcheng, Yuxin Wang, Chi He, Ning Liu, Yiqiong Yang, Yin Wang, Chem.-A Eur. J. 24 (2018) 8822–8832.
[2] Chi He, Zeyu Ji ng, Mudi Ma, Xiaodong Zh ng, Mark Douthwaite, Jian-Wen Shi, Zhengping Hao, ACS Catal. 8 (2018) 4213–4229.
[3] Hossein Ebrahimzade, Gholam Reza Khayati, Mahin Schaffie, H. Ebrahimzade, G.R. Khayati, Schaffie, J. Environ. Chem. Eng. 6 (2018) 3999–4007.
[ ] H. Chen, J. He, C. Zhang, H. He, J. Phys. Chem. C 111 (2007) 18033–18038.
[5] A.K. Sinha, M. Pradhan, T. Pal, J. Phys. Chem. C 117 (2013) 23976–23986.
[6] Hasinur Rahaman, Sujit Kumar Ghosh, RSC Adv. 6 (2016) 4531.
[ ] Xiaodong Zhang, Hongxin Li, Fulin Hou, Yang Yang, Han Dong, Ning Liu, Yuxin Wang, Lifeng Cui, Appl. Surf. Sci. 411 (2017) 27–33.
[8] Yu. Ding, A. Changjun Hou, B. Baikun Li, C. Yu Lei, Electroanalysis 23 (2011) 1245–1255.
[9] Trung Dung Dang, Thi Thu Hang Le, Thi Bich Thuy Hoang, Thanh Tung Mai, Adv. Nat. Sci. Nanosci. Nanotechnol. 6 (2015) 2.
[10] X. Zhang, Y. Yang, L. Song, J. Chen, Y. Yang, Y. Wang, J. Hazard. Mater. (2018), https://doi.org/10.1016/j.jhazmat.2018.11.049.
[11] X. Zhang, Y. Yang, L. Song, Y. Wang, C. He, Z. Wang, L. Cui, Mol. Catal. 447 (2018) 80–89.
[12] X. Zhang, X. Zhang, L. Song, F. Hou, Y. Yang, Y. Wang, N. Liu, Int. J. Hydrogen Energy 43 (2018) (2018) 18279–18288.
[13] N. Liu, W. Huang, M. Tang, C. Yin, B. Gao, Z. Li, X. Zhang, Chem. Eng. J. (2018), https://doi.org/10.1016/j.cej.2018.11.143.
[14] Manuel Bañobre-López, M. Lorena García-Hevia, Fatima Cerqueira, Francisco Rivadulla, Juan Gallo, Chem. A Europ. J. 24 (2018) 1295–1303.
[15] R. Nikam, S. Rayaprol, P.S. Goyal, P.D. Babu, S. Radha, V. Siruguri, J. Super, Novel Mag. 31 (2018) 2179–2185.
[16] S. Rayaprol, S.D. Kaushik, Cer. Inter. 41 (2015) 9567–9571.
[17] X. Fang, X. Lu, X. Guo, Y. Mao, Y.-S. Hu, J. Wang, Z. Wang, F. Wu, H. Liu, L. Chen, Electrochem. Commun. 12 (2010) 1520–1523.
[18] W.S. Seo, H.H. Jo, K. Lee, B. Kim, S.J. Oh, J.T. Park, Angew. Chem. Int. Ed. 43 (2004) 1115–1117.
[19] Du. Jin, Yongqian Gao, Lanlan Chai, Guifu Zou, Yue Li, Yitai Qian, Nanotechnology 17 (2006) 4923–4928.
[20] I.K. Gopalakrishnan, N. Bagkar, R. Ganguly, S.K. Kulshreshtha, J. Crys. Growth. 280 (2005) 436–441.
[21] Y. Wang, L. Zhu, X. Yang, E. Shao, X. Deng, N. Liu, M. Wu, J. Mater. Chem. A. 3 (2015) 2934-294.
[22] M. Anilkumar, V. Ravi, Mat. Res. Bull. 40 (2005) 605–609.
[23] Samaneh Ramezanpour, Iran Sheikhshoaie, Massumeh Khatamian, J. Mole. Liq. 231 (2017).
[24] H Hossieni Morsali, A Morsali Monfared, J. Mol. Str. 938 (2009) 10–14.
[25] Matthias Augustin, Daniela Fenske, Ingo Bardenhagen, Anne Westphal, Martin Knipper, Thorsten Plaggenborg, Joanna Kolny-Olesiak, Jürgen Parisi, Beilstein J. Nanotechnol. 6 (2015) 47–59.
[26] A.K.M. Atique Ullah, A.K.M. Fazle Kibria, M. Akter, M.N.I. Khan, M.A. Maksud, Rumana A. Jahan, Shakhawat H. Firoz, J. Saudi Chem. Soc. 21 (2017) 830–836.
[27] V. Jagadeesha Angadi, A.V. Anupama, Harish K. Choudhary, R. Kumar, H.M. Somashekarappa, M. Mallappa, B. Rudraswamy, B. Sahoo, J. Solid State Chem. 246 (2017) 119–124.
[28] I.S. Jacobs, J. Phys. Chem. Solids. 11 (1959) 1.